Supporting Information

Huang et al. 10.1073/pnas.1712297114

SI Materials and Methods

Protein Expression and Purification. Isotopically labeled α_7 (Δ97–103, referred to as WT in the text) samples (both WT and mutants discussed in the text) were expressed and purified as previously described (23, 54). All α_7-mutants, except for protomers with the Gly-rich gate, were prepared with *PftTurbo* DNA polymerase using the QuikChange site-directed mutagenesis method. The Gly-rich gate α_7-construct was prepared with *NEB* Gibson Assembly Master Mix using the Gibson assembly approach (55). All NMR samples were highly deuterated by expression in M9 minimal media, 99% D_2O, with d_7-glucose as the sole carbon source. Selective methyl labeling was achieved as previously described (56, 57) by adding one or more of the following: 100 mg/L [$\varepsilon^{13}CH_3$]-methionine (CLM-206; Cambridge Isotope Laboratories) for Met labeling, 60 mg/L α-ketobutyric acid (CDLM-7318; Cambridge Isotope Laboratories) for labeling as δ-[$^{13}CH_3$]-Ile, and 100 mg/L α-ketoisovaleric acid (CDLM-7317; Cambridge Isotope Laboratories) for labeling γ/δ-[$^{13}CH_3$,$^{12}CD_3$]-Val/Leu. All precursors were added 1 h before the induction of protein overexpression using 1 mM IPTG (OD_{600} ~ 0.8, expression at 25 °C overnight). All proteins (except for gateless α_7) were purified on a Ni affinity column (GE Healthcare), followed by cleavage of the purification tag using tobacco etch virus protease and gel filtration (54). Gateless α_7 (Δ12-α_7 and Δ12-α_7 F91R), containing a C-terminal uncleavable His_6-tag, was dialyzed into 50 mM Tris (pH 7.5), 1 mM EDTA, and 2 mM DTT buffer after Ni purification, and directly subjected to gel filtration. Before NMR experiments were recorded, proteins were exchanged into NMR buffer containing 25 mM potassium phosphate (pH 7.5), 50 mM sodium chloride, 0.03% azide, 1 mM EDTA, and 99.9% D_2O using a centrifugal concentrator (50-kDa molecular mass cutoff). The 11S regulator from *Trypanosoma brucei* (PA26) was expressed and purified as previously described (35).

Reconstitution of α_7-Rings. To prepare reconstituted α_7-rings, we have developed a protocol in which two types of purified α_7-rings (for example, PWT and gateless) are mixed at an intended molar ratio, concentrated using a centrifugal concentrator (50-kDa molecular mass cutoff) to ~250 μL, and then dissolved in 4 mL of an unfolding buffer containing 50 mM sodium phosphate (pH 7.4), 100 mM sodium chloride, 2 mM DTT, and 6 M guanidinium hydrochloride. Refolding was achieved via 15-fold fast-dilution of the unfolded mixture of α-subunits (4 mL) into refolding buffer [60 mL; 50 mM sodium phosphate (pH 7.5), 100 mM sodium chloride, and 2 mM DTT]. The refolded product was then subjected to gel filtration to obtain reconstituted α_7-rings before a final buffer exchange step prior to recording NMR experiments. The molar composition of the two components in the NMR samples was determined by electrospray ionization mass spectrometry. Unlabeled α-subunits (for each of the two protomer constituents of the rings) were used as internal standards to correct the difference in ionization efficiency of the two constructs.

Spin Labeling. Labeling of α-subunits with a nitroxide spin label was achieved by introducing a single Cys mutant at position −2 (A-2C) or position 2 (G2C). Before attaching the spin label, purified ILVM-methyl–labeled Cys α-mutant and gateless α_7 were reconstituted into α_7-rings with a molar ratio of 1:4, as described in the text. The reconstituted α_7-rings were stored with 5 mM DTT and subsequently exchanged into 1–2 mL of 50 mM sodium phosphate (pH 7.5), 100 mM sodium chloride buffer immediately before the spin label addition. 3-(2-Iodoacetamido)-proxyl spin label (Toronto Research Chemicals) was added in fivefold molar access, and the reaction was allowed to occur overnight at 25 °C. The reaction was terminated by exchange into NMR buffer. The correct labeling was confirmed via mass spectrometry; spin labels were not attached to the native C151. Reduced samples were generated through direct addition of 100 mM ascorbic acid and left at 4 °C overnight, followed by exchange into NMR buffer.

NMR Experiments, Data Processing, and Analysis. Translational diffusion coefficients for α_7-rings and the α_7–11S complex were measured at 25 °C. A series of ^{13}C-edited 1D ^{1}H spectra with nine different gradient strengths varying from 4.5 to 40.5 G/cm were recorded using a pulse scheme that is similar to an ^{15}N-edited experiment published previously with ^{15}N and ^{13}C pulses interchanged (39). A constant diffusion delay of 300 ms was used, and the duration of encoding/decoding gradients was set to 1.5 ms. The resulting ^{1}H signal was integrated over the ^{1}H frequency range of Met methyl groups to obtain intensity I, and the diffusion coefficient D was obtained by fitting I as a function of the square of the gradient-encoding pulses G^2 using the relation $I = I_0 \exp(-ADG^2)$, where I_0 is the peak intensity in the absence of gradient G and A is a constant that depends on the experimental parameters.

To correct for differential magnetization losses from ^{1}H transverse relaxation during fixed periods in the HMQC experiment, ^{1}H R_2 rates of the *in* and *out* resonances (M-1) were measured using a modified 2D ^{13}C–^{1}H HMQC experiment (50 °C), which included a chemical shift and scalar coupling refocused relaxation delay immediately before recording ^{1}H magnetization (t_2). Five relaxation delays ranging from 2 to 20 ms were used, with $\Delta R_2 = R_{2,in} - R_{2,out} = 28.4\ s^{-1}$ for M-1 of the PWT α_7-rings, 37.4 s^{-1} for M-1 of Y8G/D9G α_7-rings, and 24.9 s^{-1} for the WT gate in the 20S CP. The fractional population of *in* gates was then calculated as $I_{in}/[I_{in} + I_{out} \exp(-\Delta R_2 T)]$, where I_{in} and I_{out} are volumes of the peaks derived from the *in* and *out* states of M-1, respectively, and T is the total duration of the magnetization transfer steps in the HMQC experiment during which ^{1}H magnetization is in the transverse plane (7.2 ms). Note that I_{in} is calculated as the sum of intensities from the pair of *in* peaks. Essentially identical ^{1}H T_2 values were measured from both of these peaks.

All datasets were processed and analyzed with NMRPipe (58) or NMRGlue (53), and visualized using NMRDraw (58) or Sparky (59). Fits of titration data to each of the two models discussed in the text and below were performed with in-house written Python scripts (available upon request), and errors in extracted probabilities were estimated by a Monte Carlo error analysis (60) involving 1,000 iterations of fitting simulated datasets.

SI Text

In what follows, we present the mathematical framework for the models that have been used to describe the titration data of Figs. 3 and 5, and Figs. S3 and S4. We consider two models from which the extracted probability values for gate entry provide insight into whether proteasome gating is cooperative. In the first (*Model 1*), the probability of a gate entering the lumen depends only on the number of gates that are already in the *in* state, with no more than two or three gates allowed in at any time (see below). There is no explicit

inclusion of interactions between adjacent gates. In the second model (*Model 2*), the conformations of the gates that are immediately adjacent to the gate in question (up to two gates) are explicitly assumed to affect the probability of the gate entering the lumen through interactions involving the *out* states. Thus, the two models are fundamentally different, as discussed in more detail below, in that gating probabilities depend on the number of gates *in* (*Model 1*) or *out* (*Model 2*) of the proteasome lumen. A consistent picture obtained from fits of titration data to both models provides, therefore, more confidence in conclusions about gating cooperativity.

As described in detail in the text, during the course of the titration, the fraction of gate-containing protomers increases, so that at any given titration point a range of α_7-particles are present, each with different numbers and configurations of gates. This is indicated in Scheme **S1**, where white and black circles denote gateless and gate-containing α-subunits, respectively. In what follows below, it will be useful to recall that the fraction of α_7-rings composed of m gates reconstituted from m gate-containing and (7-m) gateless rings can be calculated as $\binom{7}{m}P_G^m(1-P_G)^{7-m}$, where P_G is the fraction of gate-containing rings in the mixture and $\binom{7}{m}=7!/[(7-m)!m!]$.

Model 1

In this model, we assume that (*i*) the probability of a gate entering the lumen, P_i^{in}, is independent of the configuration (arrangement) of the gates in the α_7-ring and is not a function of m. For example, for $m = 3$ and $m = 4$ in Scheme **S1**, there are five different gating configurations and a given P_i^{in} value is assumed to be the same for each of the five. We do not assume, in the most general case, that the probability of each gate entering the lumen is the same, however, so that P_1^{in}, P_2^{in}, and P_3^{in} may all be different. In the case where all P_i^{in} values are similar, then there is little gating cooperativity as the entry of gate j into the proteasome lumen is not influenced significantly by the fact that gate j-1 has already entered. When $P_{i+1}^{in} >(<) P_i^{in}$ for all i, then gating is positively (negatively) cooperative. (*ii*) Probability values are only affected by the number of *in* gates that have already entered the proteasome lumen. (*iii*) The pore size of the α-annulus is such that M^{in} is either 2 or 3.

In what follows, we denote a gate G_i in the *in* conformation as $G_i = 1$ and in the *out* conformation as $G_i = 0$, with the probabilities for a gate adopting the *in* conformation given that 0, 1, or 2 other gates are already *in* as a, b, and c that correspond to P_1^{in}, P_2^{in}, and P_3^{in}, respectively, in the main text. This assumes that $M^{in} = 3$, but as discussed in the text $M^{in} = 2$ is just a special case of $M^{in} = 3$ with $c = 0$. We use canonical notations for conditional probability whereby $P(A|B)$ refers to the probability of event A occurring assuming condition B. Thus, $P(G_i=1|G_j=0,G_k=0,G_l=0)$ is the probability of gate i adopting the *in* conformation given that the three other gates (j, k, l) are *out* in an α_7-ring containing four protomers with gates (and three without). The value of M^{in} leads to a set of conditional probability equations that can be solved to obtain the probabilities of each α_7-gating configuration (Scheme **S1**) and hence the expected numbers of *in* and *out* gates for a given P_G value. Below, we show an example for the case of an α_7-ring with a total number of four gates, $m = 4$ (species 4–1 through to 4–5 in Scheme **S1**), for $M^{in} = 3$.

The conditional probabilities that are germane to the problem are given by the following:

$$\begin{aligned}
&P(G_i=1|G_j=0,G_k=0,G_l=0)=a\\
&P(G_i=1|G_j=1,G_k=0,G_l=0)=b\\
&P(G_i=1|G_j=1,G_k=1,G_l=0)=c\\
&P(G_i=1|G_j=1,G_k=1,G_l=1)=0,
\end{aligned} \qquad \textbf{[S1]}$$

and the goal is to calculate the following probabilities:

$$\begin{aligned}
&P_{0000}=P(G_i=0,G_j=0,G_k=0,G_l=0)\\
&P_{1000}=P(G_i=1,G_j=0,G_k=0,G_l=0)=P_{0100}=P_{0010}=P_{0001}\\
&P_{1100}=P(G_i=1,G_j=1,G_k=0,G_l=0)=P_{1010}=P_{1001}=P_{0110}=P_{0101}=P_{0011}\\
&P_{1110}=P(G_i=1,G_j=1,G_k=1,G_l=0)=P_{1101}=P_{1011}=P_{0111}\\
&P_{1111}=0.
\end{aligned} \qquad \textbf{[S2]}$$

It is important to note that, in this model (as stated above) and made clear in Eq. **S2**, the probability of each configuration with the same number of *in* gates is the same (for example, $P_{1000} = P_{0100}\ldots$). It follows that

$$\begin{aligned}
&P_{0000}=P(G_i=0|G_j=0,G_k=0,G_l=0)\cdot P(G_j=0,G_k=0,G_l=0)=(1-a)P_{000}\\
&P_{1000}=P(G_i=1|G_j=0,G_k=0,G_l=0)\cdot P(G_j=0,G_k=0,G_l=0)=aP_{000}\\
&P_{0100}=P(G_i=0|G_j=1,G_k=0,G_l=0)\cdot P(G_j=1,G_k=0,G_l=0)=(1-b)P_{100}\\
&P_{1100}=P(G_i=1|G_j=1,G_k=0,G_l=0)\cdot P(G_j=1,G_k=0,G_l=0)=bP_{100}\\
&P_{0110}=P(G_i=0|G_j=1,G_k=1,G_l=0)\cdot P(G_j=1,G_k=1,G_l=0)=(1-c)P_{110}\\
&P_{1110}=P(G_i=1|G_j=1,G_k=1,G_l=0)\cdot P(G_j=1,G_k=1,G_l=0)=cP_{110}\\
&P_{0111}=P(G_i=0|G_j=1,G_k=1,G_l=1)\cdot P(G_j=1,G_k=1,G_l=1)=P_{111},
\end{aligned} \qquad \textbf{[S3]}$$

from which the following relations are obtained:

$$\begin{aligned}
&aP_{000}=(1-b)P_{100}\\
&bP_{100}=(1-c)P_{110}\\
&cP_{110}=P_{111},
\end{aligned} \qquad \textbf{[S4]}$$

where P_{ijk} and P_{ijkl} in Eqs. **S2** and **S3** are subject to the following constraints:

$$P_{000} + 3P_{100} + 3P_{110} + P_{111} = 1$$
$$P_{0000} + 4P_{1000} + 6P_{1100} + 4P_{1110} = 1. \quad \textbf{[S5]}$$

From Eqs. **S1**–**S5**, it can be shown that

$$P_{0000} = \frac{(1-a)(1-b)(1-c)}{D}$$
$$P_{1000} = \frac{a(1-b)(1-c)}{D}$$
$$P_{1100} = \frac{ab(1-c)}{D} \quad \textbf{[S6]}$$
$$P_{1110} = \frac{abc}{D},$$

where $D = (1-a)(1-b)(1-c) + 4a(1-b)(1-c) + 6ab(1-c) + 4abc$. Thus, given an α_7-ring with $m = 4$ gate-containing protomers, the probability of rings with 0, 1, 2, and 3 gates in the *in* position is as follows:

$$P_{0,4} = P_{0000}$$
$$P_{I,4} = 4P_{1000}$$
$$P_{II,4} = 6P_{1100} \quad \textbf{[S7]}$$
$$P_{III,4} = 4P_{1110},$$

and the number of gates per ring that are *in* (E_4^{in}) and *out* (E_4^{out}) is as follows:

$$E_4^{in} = P_{I,4} + 2P_{II,4} + 3P_{III,4}$$
$$E_4^{out} = 4P_{0,4} + 3P_{I,4} + 2P_{II,4} + P_{III,4}. \quad \textbf{[S8]}$$

The analysis given above can be repeated for any m, $1 \le m \le 7$, and the values of $P_{0,\mathrm{m}}$, $P_{I,\mathrm{m}}$, $P_{II,\mathrm{m}}$, and $P_{III,\mathrm{m}}$ calculated as before:

i) $m = 1$,

$$P_{0,1} = 1 - a$$
$$P_{I,1} = a \quad \textbf{[S9]}$$
$$P_{II,1} = P_{III,1} = 0;$$

ii) $m = 2$,

$$P_{0,2} = \frac{(1-a)(1-b)}{D}$$
$$P_{I,2} = \frac{2a(1-b)}{D} \quad \textbf{[S10]}$$
$$P_{II,2} = \frac{ab}{D}$$
$$P_{III,2} = 0,$$

where $D = 1 + a - b$.

iii) $m \ge 3$,

$$P_{0,m} = \binom{m}{0} \frac{(1-a)(1-b)(1-c)}{D}$$
$$P_{I,m} = \binom{m}{1} \frac{a(1-b)(1-c)}{D} \quad \textbf{[S11]}$$
$$P_{II,m} = \binom{m}{2} \frac{ab(1-c)}{D}$$
$$P_{III,m} = \binom{m}{3} \frac{abc}{D},$$

with $D = (1-a)(1-b)(1-c) + \binom{m}{1} a(1-b)(1-c) + \binom{m}{2} ab(1-c) + \binom{m}{3} abc$.

The effective (average) number of *in* and *out* gates per ring is given by the following:

$$\sum_{m=1}^{7}\binom{7}{m}P_G^m(1-P_G)^{7-m}E_m^{in}$$
$$\sum_{m=1}^{7}\binom{7}{m}P_G^m(1-P_G)^{7-m}E_m^{out}, \quad \textbf{[S12]}$$

respectively, where

$$E_m^{in}=P_{I,m}+2P_{II,m}+3P_{III,m}$$
$$E_m^{out}=mP_{0,m}+(m-1)P_{I,m}+(m-2)P_{II,m}+(m-3)P_{III,m}. \quad \textbf{[S13]}$$

Finally, the fractional populations of *in* and *out* gates is simply the following:

$$P_{in}=\left(\frac{1}{7P_G}\right)\sum_{m=1}^{7}\binom{7}{m}P_G^m(1-P_G)^{7-m}E_m^{in}$$
$$P_{out}=\left(\frac{1}{7P_G}\right)\sum_{m=1}^{7}\binom{7}{m}P_G^m(1-P_G)^{7-m}E_m^{out}. \quad \textbf{[S14]}$$

Note that, although this derivation assumes $M^{in}=3$, the corresponding equations for the case where $M^{in}=2$ can be readily obtained by setting $c=0$ in the above expressions.

Finally, although it is possible to generalize the results of this section for any M^{in} value, we have not fit our data to models with $M^{in}>3$. Molecular modeling suggests that the size of the annulus (Fig. 1*B*) is such that no more than three gates will be allowed in the lumen simultaneously.

Model 2

In this model, we explicitly include the possibility of interactions between neighboring *out* gates. This model is motivated by the X-ray structure of the 11S-bound proteasome (PDB ID code 1YA7) showing contacts between Tyr8 and Asp9 from adjacent protomers (14). Whether such interactions are present in the context of the naked proteasome, leading potentially to gating cooperativity, is not known a priori. In this model (*i*) the probability of a gate adopting the *in* conformation depends on the number of immediately adjacent *out* gates where $\tilde{P}_0$, $\tilde{P}_1$, and $\tilde{P}_2$ are the probabilities of a gate adopting the *in* state when it has 0, 1, or 2 *out* neighbors (see below). For the case where $\tilde{P}_0\sim\tilde{P}_1\sim\tilde{P}_2$, gating is noncooperative as entry of a gate into the lumen is little affected by the status of surrounding gates, while if $\tilde{P}_1\sim\tilde{P}_2=0$ gating is completely cooperative as the probability of a gate entering the lumen is fully dependent on the *out* status of the immediately neighboring gates; (*ii*) having no neighboring gates is equivalent to having 0 *out* neighbors (i.e., no interactions with adjacent gates); (*iii*) the pore size of the α-annulus limits M^{in} to either 2 or 3; (*iv*) as shown below, $\{\tilde{P}_0,\tilde{P}_1,\tilde{P}_2\}$ are interrelated so that if $\tilde{P}_0=\tilde{P}_1$, then it follows that $\tilde{P}_0=\tilde{P}_1=\tilde{P}_2$ (Eq. **S22**).

As before, in what follows, we denote a gate G_i in the *in* conformation as $G_i=1$ and in the *out* conformation as $G_i=0$. Thus, we obtain the following:

$$P(G_i=1|G_{i-1}=1,G_{i+1}=1)=\tilde{P}_0\left(M^{in}=3\right),=0\left(M^{in}=2\right)$$
$$P(G_i=1|G_{i-1}=1,G_{i+1}=0)=\tilde{P}_1$$
$$P(G_i=1|G_{i-1}=0,G_{i+1}=1)=\tilde{P}_1$$
$$P(G_i=1|G_{i-1}=0,G_{i+1}=0)=\tilde{P}_2. \quad \textbf{[S15]}$$

In the case of an α_7-ring containing m gates, each configuration could be treated identically for model 1 because interactions between adjacent gates were not explicitly considered. By contrast, for model 2, each of the gate distributions for a given m must be considered separately because this model takes into account nearest neighbor gate interactions. For example, for $m=3$ (Scheme **S1**, fourth row), there are five possible configurations (3–1 to 3–5), of which 3–2, 3–3, and 3–4 are degenerate (two adjacent gates separated by at least one gateless protomer on either side), leaving three distinct cases to be computed separately. As an example, we compute E_3^{in} and E_3^{out} values for the 3–1 configuration, below, assuming $M^{in}=2$ (where the gates are numbered as shown in Scheme **S1** for the particular case under evaluation).

From the assumptions above, and following along the lines of Eq. **S15**, it can be shown that ($M^{in} = 2$):

$$\begin{aligned}
&P(G_1=1|G_2=1,G_3=1)=0\\
&P(G_1=1|G_2=1,G_3=0)=\tilde{P}_0\\
&P(G_1=1|G_2=0,G_3=0)=P(G_1=1|G_2=0,G_3=1)=\tilde{P}_1\\
&P(G_2=1|G_1=1,G_3=1)=0\\
&P(G_2=1|G_1=0,G_3=1)=P(G_2=1|G_1=1,G_3=0)=\tilde{P}_1\\
&P(G_2=1|G_1=0,G_3=0)=\tilde{P}_2\\
&P(G_3=1|G_1=1,G_2=1)=0\\
&P(G_3=1|G_1=0,G_2=1)=\tilde{P}_0\\
&P(G_3=1|G_1=1,G_2=0)=P(G_3=1|G_1=0,G_2=0)=\tilde{P}_1,
\end{aligned} \tag{S16}$$

which we will subsequently use to calculate the probabilities $P_{ijk} = P(G_1 = i, G_2 = j, G_3 = k)$. This is achieved as follows:

$$\begin{aligned}
P_{100}&=P(G_1=1|G_2=0,G_3=0)\cdot P(G_2=0,G_3=0)\\
&=\tilde{P}_1\cdot(P_{000}+P_{100})\\
\therefore P_{100}&=\frac{\tilde{P}_1}{1-\tilde{P}_1}P_{000},
\end{aligned} \tag{S17}$$

and from symmetry,

$$P_{001}=P_{100}=\frac{\tilde{P}_1}{1-\tilde{P}_1}P_{000}. \tag{S18}$$

Similarly, it follows that

$$P_{010}=\frac{\tilde{P}_2}{1-\tilde{P}_2}P_{000}. \tag{S19}$$

We can also calculate P_{110}, P_{011}, and P_{101} in terms of P_{000}:

$$\begin{aligned}
P_{110}&=P(G_1=1|G_2=1,G_3=0)\cdot P(G_2=1,G_3=0)\\
&=\tilde{P}_0\cdot(P_{010}+P_{110})\\
\therefore P_{110}&=\frac{\tilde{P}_0}{1-\tilde{P}_0}P_{010}=\frac{\tilde{P}_0\tilde{P}_2}{\left(1-\tilde{P}_0\right)\left(1-\tilde{P}_2\right)}P_{000},
\end{aligned} \tag{S20}$$

where we have made use of Eq. **S19**. However, P_{110} can also be calculated as follows:

$$\begin{aligned}
P_{110}&=P(G_2=1|G_1=1,G_3=0)\cdot P(G_1=1,G_3=0)\\
&=\tilde{P}_1\cdot(P_{100}+P_{110})\\
\therefore P_{110}&=\frac{\tilde{P}_1}{1-\tilde{P}_1}P_{100}=\frac{\tilde{P}_1^2}{\left(1-\tilde{P}_1\right)^2}P_{000},
\end{aligned} \tag{S21}$$

where Eq. **S17** has been used. Comparing Eqs. **S20** and **S21**, it follows that

$$\frac{\tilde{P}_0\tilde{P}_2}{\left(1-\tilde{P}_0\right)\left(1-\tilde{P}_2\right)}=\frac{\tilde{P}_1^2}{\left(1-\tilde{P}_1\right)^2}, \tag{S22}$$

so that $\tilde{P}_0$, $\tilde{P}_1$, and $\tilde{P}_2$ are not mutually independent. Finally, it is straightforward to show that $P_{110}=P_{101}=P_{011}$, and $P_{111} = 0$, since $M^{in} = 2$.

P_{ijk} values can be calculated by noting that $\sum P_{ijk} = 1$, and since P_{ijk} values are written in terms of P_{000} above, it follows that

$$P_{000} = \frac{1}{1 + 2q_1 + q_2 + 3q_1^2}, \qquad \textbf{[S23]}$$

where $q_i = \tilde{P}_i/(1 - \tilde{P}_i)$. All other P_{ijk} values can be derived directly from Eq. **S23** using Eqs. **S17–S21** above. Thus, the number of *in* and *out* gates (per ring) for configuration 3–1 of Scheme **S1** is given by the following:

$$\begin{aligned} E_{3-1}^{in} &= \frac{2q_1 + q_2 + 2 \cdot 3q_1^2}{1 + 2q_1 + q_2 + 3q_1^2} \\ E_{3-1}^{out} &= \frac{3 + 4q_1 + 2q_2 + 3q_1^2}{1 + 2q_1 + q_2 + 3q_1^2}. \end{aligned} \qquad \textbf{[S24]}$$

Following the same strategy as above, we can calculate $E_{m-\text{config}_i}^{in}$ and $E_{m-\text{config}_i}^{out}$ for each m value and configuration ($config_i$) and sum over all configurations for a given m to obtain the following list of E_m^{in} values for the case where $M^{in} = 2$:

$$E_m^{in} = \begin{cases} 0, & m = 0 \\ \tilde{P}_0, & m = 1 \\ 2 - \dfrac{4q_0 + 4}{3(q_0^2 + 2q_0 + 1)} - \dfrac{2q_1 + 2}{3(q_0q_1 + 2q_1 + 1)}, & m = 2 \\ 3 - \dfrac{9q_0q_1 + 6q_0 + 12q_1 + 9}{5(3q_0q_1 + q_0 + 2q_1 + 1)} - \dfrac{3q_1^2 + 4q_1 + 2q_2 + 3}{5(3q_1^2 + 2q_1 + q_2 + 1)} & m = 3 \\ \quad - \dfrac{3q_0^2 + 6q_0 + 3}{5(3q_0^2 + 3q_0 + 1)}, & \\ 4 - \dfrac{8q_0q_1 + 4q_0q_2 + 6q_0 + 12q_1^2 + 12q_1 + 6q_2 + 8}{5(2q_0q_1 + q_0q_2 + q_0 + 3q_1^2 + 2q_1 + q_2 + 1)} & m = 4 \\ \quad - \dfrac{6q_1^2 + 6q_1q_2 + 6q_1 + 6q_2 + 4}{5(3q_1^2 + 3q_1q_2 + 2q_1 + 2q_2 + 1)} - \dfrac{2q_0^2 + 10q_0q_1 + 6q_0 + 6q_1 + 4}{5(q_0^2 + 5q_0q_1 + 2q_0 + 2q_1 + 1)} & \\ \quad - \dfrac{4q_0q_1 + 8q_1^2 + 12q_1 + 4}{5(2q_0q_1 + 4q_1^2 + 4q_1 + 1)}, & \\ 5 - \dfrac{6q_0q_1 + 6q_0q_2 + 4q_0 + 9q_1^2 + 9q_1q_2 + 8q_1 + 8q_2 + 5}{3(2q_0q_1 + 2q_0q_2 + q_0 + 3q_1^2 + 3q_1q_2 + 2q_1 + 2q_2 + 1)} & m = 5 \\ \quad - \dfrac{3q_0q_1 + 21q_1^2 + 6q_1q_2 + 16q_1 + 4q_2 + 5}{3(q_0q_1 + 7q_1^2 + 2q_1q_2 + 4q_1 + q_2 + 1)} & \\ \quad - \dfrac{9q_1^2 + 18q_1q_2 + 8q_1 + 3q_2^2 + 12q_2 + 5}{3(3q_1^2 + 6q_1q_2 + 2q_1 + q_2^2 + 3q_2 + 1)}, & \\ 6 - \dfrac{12q_1^2 + 36q_1q_2 + 10q_1 + 12q_2^2 + 20q_2 + 6}{3q_1^2 + 9q_1q_2 + 2q_1 + 3q_2^2 + 4q_2 + 1}, & m = 6 \\ 7 - \dfrac{35q_1q_2 + 70q_2^2 + 42q_2 + 7}{7q_1q_2 + 14q_2^2 + 7q_2 + 1}, & m = 7 \end{cases} \qquad \textbf{[S25]}$$

and for $M^{in} = 3$,

$$E_m^{in} = \begin{cases} 0, & m=0 \\ \tilde{P}_0, & m=1 \\ 2-\dfrac{4q_0+4}{3\left(q_0^2+2q_0+1\right)}-\dfrac{2q_1+2}{3\left(q_0q_1+2q_1+1\right)}, & m=2 \\ 3-\dfrac{3q_0^2+6q_0+3}{5\left(q_0^3+3q_0^2+3q_0+1\right)}-\dfrac{3q_1^2+4q_1+2q_2+3}{5\left(q_0q_1^2+3q_1^2+2q_1+q_2+1\right)} & m=3 \\ \quad -\dfrac{9q_0q_1+6q_0+12q_1+9}{5\left(q_0^2q_1+3q_0q_1+q_0+2q_1+1\right)}, & \\ 4-\dfrac{8q_0q_1^2+8q_0q_1+4q_0q_2+6q_0+12q_1^2+12q_1+6q_2+8}{5\left(4q_0q_1^2+2q_0q_1+q_0q_2+q_0+3q_1^2+2q_1+q_2+1\right)} & m=4 \\ \quad -\dfrac{4q_0^2q_1+2q_0^2+10q_0q_1+6q_0+6q_1+4}{5\left(4q_0^2q_1+q_0^2+5q_0q_1+2q_0+2q_1+1\right)}-\dfrac{4q_1^3+6q_1^2+6q_1q_2+6q_1+6q_2+4}{5\left(4q_1^3+3q_1^2+3q_1q_2+2q_1+2q_2+1\right)} & \\ \quad -\dfrac{4q_0q_1^2+4q_0q_1+8q_1^2+12q_1+4}{5\left(4q_0q_1^2+2q_0q_1+4q_1^2+4q_1+1\right)}, & \\ 5-\dfrac{6q_0q_1^2+6q_0q_1q_2+6q_0q_1+6q_0q_2+4q_0+8q_1^3+9q_1^2+9q_1q_2+8q_1+8q_2+5}{3\left(3q_0q_1^2+3q_0q_1q_2+2q_0q_1+2q_0q_2+q_0+4q_1^3+3q_1^2+3q_1q_2+2q_1+2q_2+1\right)} & m=5 \\ \quad -\dfrac{6q_0q_1^2+2q_0q_1q_2+3q_0q_1+12q_1^3+21q_1^2+6q_1q_2+16q_1+4q_2+5}{3\left(3q_0q_1^2+q_0q_1q_2+q_0q_1+6q_1^3+7q_1^2+2q_1q_2+4q_1+q_2+1\right)} & \\ \quad -\dfrac{8q_1^3+12q_1^2q_2+9q_1^2+18q_1q_2+8q_1+3q_2^2+12q_2+5}{3\left(4q_1^3+6q_1^2q_2+3q_1^2+6q_1q_2+2q_1+q_2^2+3q_2+1\right)}, & \\ 6-\dfrac{12q_1^3+36q_1^2q_2+12q_1^2+12q_1q_2^2+36q_1q_2+10q_1+12q_2^2+20q_2+6}{4q_1^3+12q_1^2q_2+3q_1^2+4q_1q_2^2+9q_1q_2+2q_1+3q_2^2+4q_2+1}, & m=6 \\ 7-\dfrac{28q_1^2q_2+72q_1q_2^2+35q_1q_2+40q_2^3+70q_2^2+42q_2+7}{7q_1^2q_2+21q_1q_2^2+7q_1q_2+7q_2^3+14q_2^2+7q_2+1}. & m=7 \end{cases} \quad \textbf{[S26]}$$

Finally, values for P_{in} and P_{out} can be calculated from Eq. **S14** with $E_m^{out} = m - E_m^{in}$.

For a given M^{in} value, models 1 and 2 converge in the limit that gates are independent. As discussed above, model 1, $M^{in} = 3$, reduces to model 1, $M^{in} = 2$, in the case where $P_3^{in} = 0$. Because $\{\tilde{P}_0, \tilde{P}_1, \tilde{P}_2\}$ of model 2 are interrelated (Eq. **S22**), it is not possible to simplify model 2 in the same way as for model 1; for both $M^{in} = 2$ and $M^{in} = 3$, there are only two fitting parameters. Thus, fits with model 2 must be performed separately with $M^{in} = 2$ and $M^{in} = 3$ in the most general case to establish whether a maximum of 2 or 3 *in* gates is consistent with the titration data.

Fits of the titration data have been carried out using models 1 and 2, as described in the main text. The fits, taken together, provide strong evidence that the gates do not interact and that the *in*/*out* movement of the gates is not cooperative.

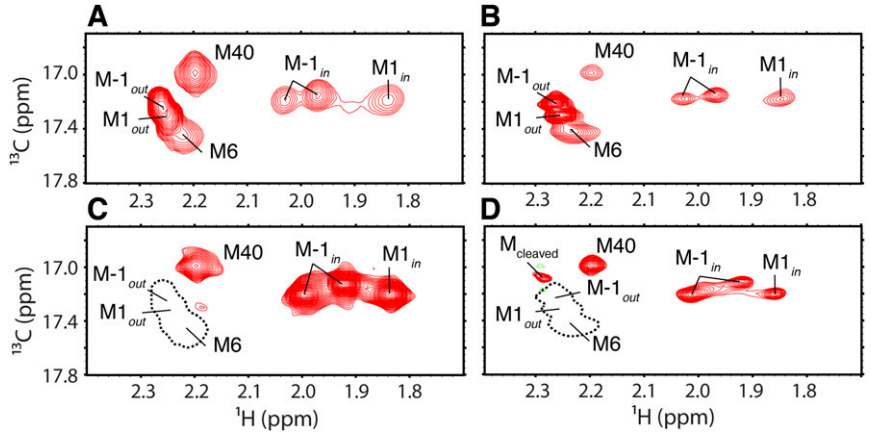

Fig. S1. WT gates in α_7 or in the full 20S CP have similar P^{in} values as PWT gates in α_7. (*A* and *B*) Selected regions from ^{13}C–^{1}H HMQC spectra recorded on samples of U-^{2}H, Met-[$\varepsilon^{13}CH_3$]–labeled WT α_7, 50 °C, 800 MHz (*A*) and {[U-^{2}H, Met- $\varepsilon^{13}CH_3$]-α, unlabeled-β} 20S CP, 70 °C, 800 MHz (*B*) from which fractional populations of *in* gates are calculated to be 29.4 ± 1.0% and 29.0 ± 0.8% for WT α_7-rings and 20S CP, respectively, compared with 28.9 ± 0.8% for *in* gates in PWT α_7-rings. The analysis of M-1 peak intensities included corrections for differential ^{1}H transverse relaxation rates. (*C* and *D*) As in *A* and *B* but for [U-^{2}H] gateless α_7-rings reconstituted with ∼5% U-^{2}H, Met-[$\varepsilon^{13}CH_3$]–labeled WT gate-containing protomers (*C*) or 20S CPs reconstituted in the same manner (*D*). Values of P^{in} were calculated to be 94.0 ± 1.4% and 96.0 ± 1.5%, respectively, compared with 95.4 ± 1.0% for the PWT gate-containing protomers that were doped into gateless rings. The dotted black single contours in *C* and *D* denote the peak positions of M-1$_{out}$, M1$_{out}$, and M6.

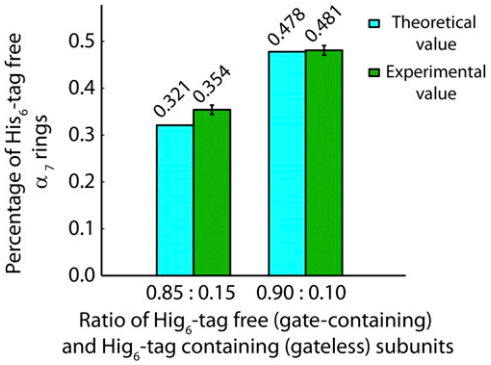

Fig. S2. Random incorporation of gate-containing and gateless subunits in α_7-rings. A fixed ratio of gate-containing and gateless subunits was used to construct α_7-rings, as described in *SI Materials and Methods*, with gate-containing subunits lacking a His_6-tag (His_6-tag free) and gateless subunits having a C-terminal His_6-tag. The resulting α_7-rings with mixed subunits were passed through a Ni affinity column, and the amount of α_7-rings in the flow-through (His_6-tag free) and bound to the Ni column (His_6-tag containing) were quantified by absorbance at 280 nM. The theoretical percentage of His_6-tag–free α_7-rings in a completely random incorporation is calculated as P_G^7, where P_G is the percentage of His_6-tag–free (gate-containing) subunits. The theoretical values agree with the experimental results, confirming the random incorporation of the two types of subunits.

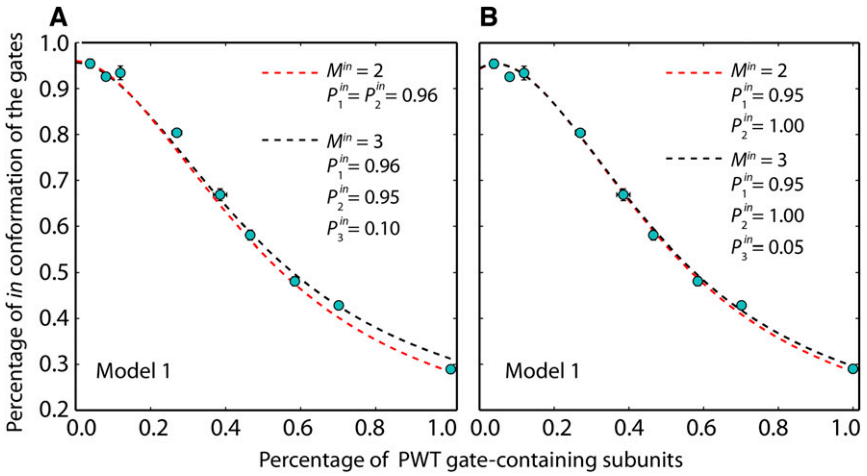

Fig. S3. (*A*) Comparison of best fits of the titration data (reconstituted α_7-rings comprising gateless subunits with an increasing proportion of PWT gate-containing subunits, circles) to model 1, $M^{in} = 2$ (red) or $M^{in} = 3$ (black), assuming $P_1^{in} = P_2^{in}$ (red fit) or $P_1^{in} = 0.96$ (black fit). (*B*) As in *A* with the exception that $\{P_1^{in}, P_2^{in}, P_3^{in}\}$ of model 1 are fit without fixing any of the values. The following best-fitted parameters were obtained: $P_1^{in} = 0.95 \pm 0.01$ and $P_2^{in} = 1.00 \pm 0.03$ for $M^{in} = 2$, and $P_1^{in} = 0.95 \pm 0.01$, $P_2^{in} = 1.00 \pm 0.02$, and $P_3^{in} = 0.05 \pm 0.03$ for $M^{in} = 3$. For comparison, values of $P_1^{in} = P_2^{in} = 0.96 \pm 0.01$ are obtained when $P_1^{in} = P_2^{in}$ ($M^{in} = 2$); $P_2^{in} = 0.95 \pm 0.02$ and $P_3^{in} = 0.10 \pm 0.03$ are obtained when $P_1^{in} = 0.96$ ($M^{in} = 3$).

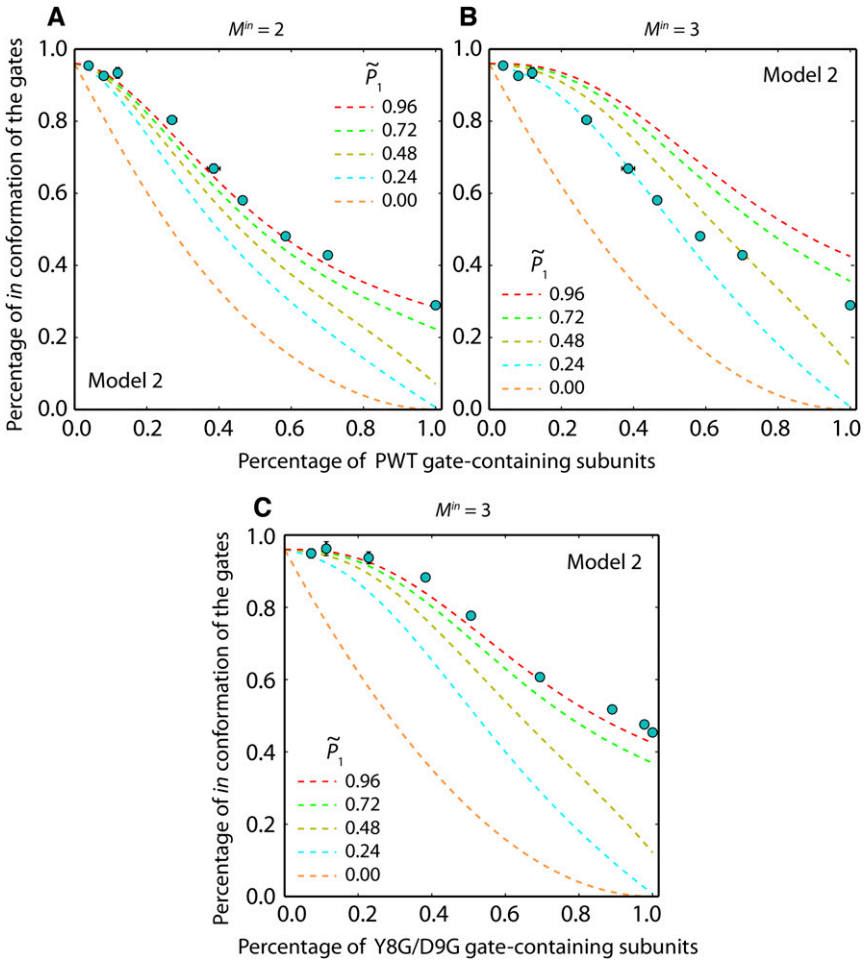

Fig. S4. Fits of titration data (reconstituted α_7-rings comprising gateless subunits with an increasing proportion of PWT gate-containing subunits, circles; see also Fig. 3*A*) to model 2. Titration curves were simulated with $M^{in} = 2$ (*A*) or $M^{in} = 3$ (*B* and *C*). The probability of a gate adopting the *in* conformation in the absence of neighboring *out* gates, $\tilde{P}_0$, is set to 0.96, as measured in the first titration point, and $\tilde{P}_1$ (*in* probability with one immediate neighboring *out* gate, $\tilde{P}_1$) was varied from 0 to 0.96, as indicated. The value of $\tilde{P}_2$ is constrained by Eq. **S22**. The data are well fit for the case of $M^{in} = 2$ (*A*, red dashed line), and the obtained $\tilde{P}_1$ strongly supports the lack of cooperativity between the gates since $\tilde{P}_0 \sim \tilde{P}_1$ (which implies that $\tilde{P}_0 \sim \tilde{P}_1 \sim \tilde{P}_2$ from Eq. **S22**). The data are not well fit assuming $M^{in} = 3$ (*B*) because a maximum of only two PWT gates occupy the lumen of the proteasome, and unlike for model 1, the $M^{in} = 3$ case does not converge to $M^{in} = 2$ when only 2 gates enter the lumen for model 2. (*C*) As in *B*, but where PWT gate-containing protomers are replaced with Y8G/D9G gate-containing subunits (circles). Note that full positive cooperativity for this model implies that $\tilde{P}_1 = 0$ (from which it also follows that $\tilde{P}_2 = 0$ for a nonzero value of $\tilde{P}_0$). It is clear that, in this case (orange dashed line), the experimental data are not fitted at all.

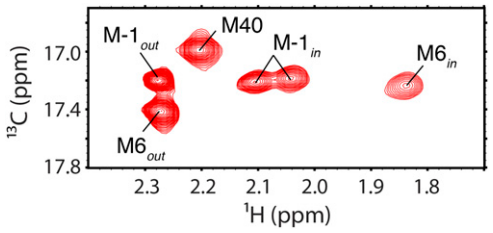

Fig. S5. Selected region of the ^{13}C–^{1}H HMQC spectrum (800 MHz, 50 °C) of U-^{2}H, Met-[$\varepsilon^{13}CH_3$]–labeled Y8G/D9G gate-containing protomers showing multiple correlations for the terminal methionine M-1 (and M6). The cross-peak intensities for M-1 (corrected for differential ^{1}H relaxation of magnetization derived from *in* and *out* conformations) are used to calculate that 45.4 ± 0.4% of the Y8G/D9G gates adopt the *in* conformation, corresponding to an average of approximately three *in* gates per α_7-ring.

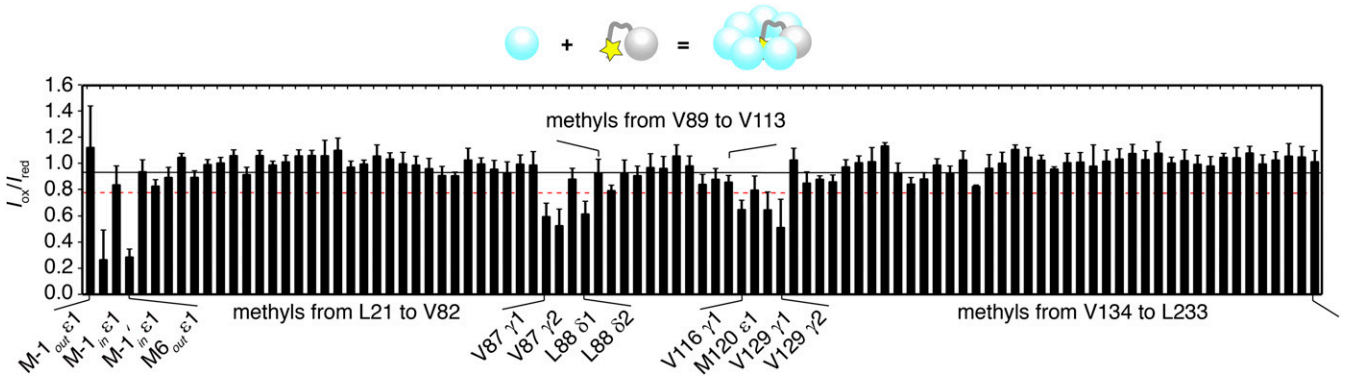

Fig. S6. PRE effect caused by a spin label attached to position 2 of the α-subunit. α_7-rings were reconstituted from a mixture of α-subunits with spin labels (gray sphere, with the yellow star representing the spin label) and gateless α-subunits (cyan spheres) at a molar ratio of 1:4. The black line indicates the average intensity ratio of a cross-peak before (I_{ox}) and after (I_{red}) the spin label is reduced, and the red dotted line denotes 1 SD below the mean. The same set of residues, including M-1, M6, V87, L88, V116, and V129, show significant PRE effects as was observed for the spin label attached to position −2 of the α-subunit (Fig. 4*A*). Note that the attachment of spin labels does not significantly alter the *in*/*out* equilibrium of the gates (see main text).

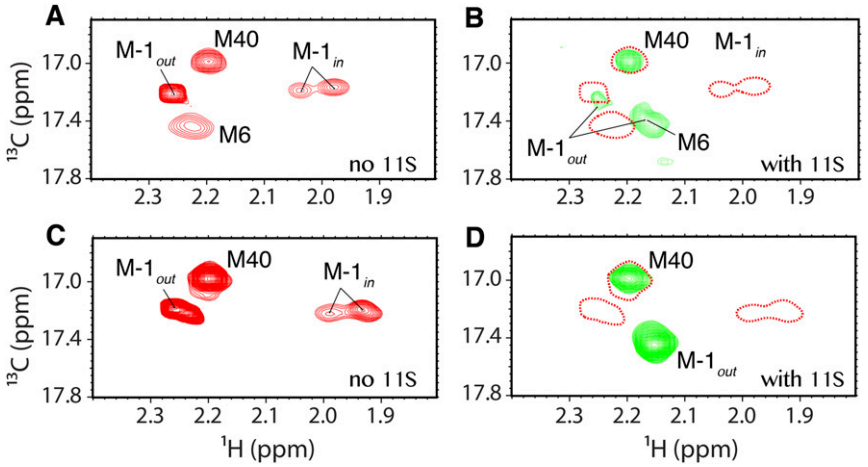

Fig. S7. Binding of the 11S regulatory particle to the PWT α_7-ring shifts the conformational equilibrium of the gates to an all-*out* state. Met regions of ^{13}C–^{1}H methyl spectra of PWT α_7 (*A* and *B*) and α_7 (M1I, M6A) (*C* and *D*) in the absence (red contours in *A* and *C*, and red dotted single contours in *B* and *D*) and presence (green contours in *B* and *D*) of 11S. The shift of the M-1_{out} peak indicates the formation of the α_7–11S complex, which is accompanied by a significant shift in the *in*/*out* equilibrium to an all-*out* state (<5% *in*).

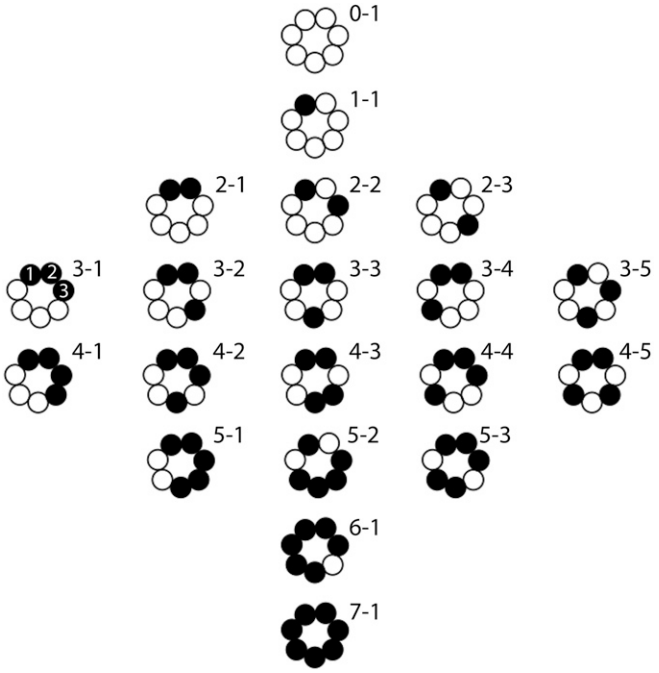

Scheme S1. Gate distributions in an α_7-ring during the course of the titrations discussed in the text. Black (white) circles represent gate-containing (gateless) subunits. Each heptameric structure corresponds to an α_7-particle. By immediate neighbors (see text, *Model 2*), we refer to protomers that are adjacent to the subunit in question. Thus, in structure 3–1, protomers 1 and 3 are immediate neighbors of protomer 2.